

Supporting Information

Sub-Ångstrom-scale structural variations in high-entropy oxides

Hanbin Gao,^{†a,b} Ning Guo,^{†b,c} Yue Gong,^{b,c} Lu Bai,^b Dongwei Wang,^b and Qiang Zheng^{*b,c}

a. Henan Institute of Advanced Technology, Zhengzhou University, Zhengzhou 450003, China.

b. CAS Key Laboratory of Standardization and Measurement for Nanotechnology, CAS Center for Excellence in Nanoscience, National Center for Nanoscience and Technology, Beijing 100190, China.

E-mail: zhengq@nanoctr.cn

c. University of Chinese Academy of Sciences, Beijing 101408, China.

† These authors contributed equally to this work.

Table S1 Crystallographic data for the four types of HEOs from refinements of their powder XRD patterns.

Samples	(Mg,Co,Ni,Cu,Zn)O	(Yb,Tb,Gd,Dy,Er) ₂ Ti ₂ O ₇	(Cr,Mn,Fe,Co,Ni) ₃ O ₄	La(Cr,Mn,Fe,Co,Ni)O ₃
Crystal system		Cubic		Orthorhombic
Space group	<i>Fm</i> ³ <i>m</i>	<i>Fd</i> ³ <i>m</i>	<i>Fd</i> ³ <i>m</i>	<i>Pbnm</i>
Lattice parameter [Å]	4.2365(2)	10.1117(2)	8.3477(3)	<i>a</i> =5.4747(2) <i>b</i> =5.5172(2) <i>c</i> =7.7542(4)
Volume [Å³]	76.034(7)	1033.88(3)	581.70(4)	234.21(2)
Calculated				
Density [g cm⁻³]	6.13	6.88	5.30	6.89
R_p	3.53%	7.42%	5.57%	8.37%
Bragg R-factor	2.83%	6.20%	7.50%	7.18%
Goodness of Fit [χ^2]	5.58	5.64	4.75	4.85

Table S2 Refined atomic coordinates for the four types of HEOs from their powder XRD patterns.

(Mg,Co,Ni,Cu,Zn)O				
atom	Wyckoff site	x	y	z
<i>M</i>	4 <i>a</i>	0	0	0
O	4 <i>b</i>	0.5	0.5	0.5
<i>M</i> = Mg, Co, Ni, Cu, and Zn with occupancy = 0.2 for each.				
(Yb,Tb,Gd,Dy,Er) ₂ Ti ₂ O ₇				
atom	Wyckoff site	x	y	z
<i>M</i>	16 <i>c</i>	0	0	0
Ti	16 <i>d</i>	0.5	0.5	0.5
O1	8 <i>a</i>	0.125	0.125	0.125
O2	48 <i>f</i>	0.4277(7)	0.125	0.125
<i>M</i> = Yb, Tb, Gd, Dy, and Er with occupancy = 0.2 for each.				
(Cr,Mn,Fe,Co,Ni) ₃ O ₄				
atom	Wyckoff site	x	y	z
<i>M1</i>	8 <i>a</i>	-0.125	-0.125	-0.125
<i>M2</i>	16 <i>d</i>	0.500	0.500	0.500
O	32 <i>e</i>	0.2597(4)	0.2597(4)	0.2597(4)
<i>M1</i> = Cr, Mn, Fe, Co, and Ni with occupancy = 0.2 for each;				
<i>M2</i> = Cr, Mn, Fe, Co, and Ni with occupancy = 0.2 for each.				
La(Cr,Mn,Fe,Co,Ni)O ₃				
atom	Wyckoff site	x	y	z
<i>M</i>	4 <i>b</i>	0.5	0	0
La	4 <i>c</i>	0.001(2)	0.0141(5)	0.25
O1	4 <i>c</i>	-0.04(1)	0.466(6)	0.25
O2	8 <i>d</i>	0.289(3)	0.282(3)	0.037(2)
<i>M</i> = Cr, Mn, Fe, Co, and Ni with occupancy = 0.2 for each.				

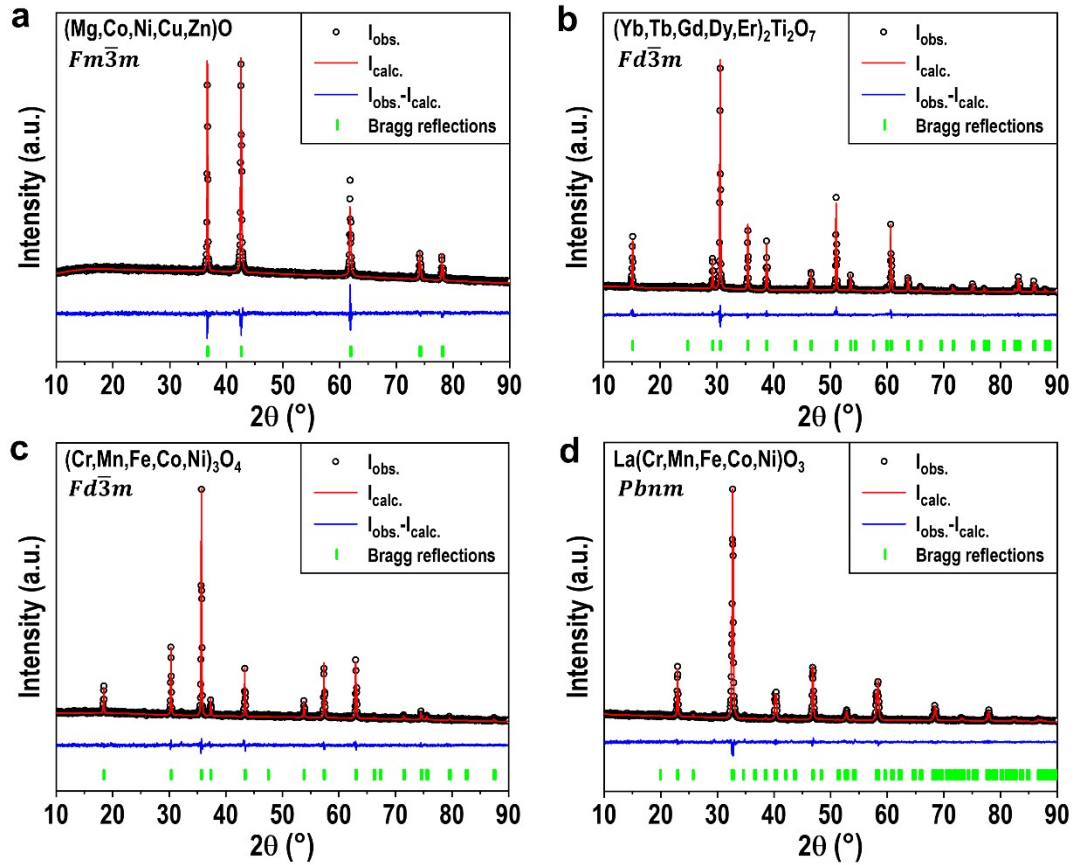


Fig. S1 XRD patterns for sintered samples of (a) rock-salt type $(\text{Mg}, \text{Co}, \text{Ni}, \text{Cu}, \text{Zn})\text{O}$, (b) pyrochlore type $(\text{Yb}, \text{Tb}, \text{Gd}, \text{Dy}, \text{Er})_2\text{Ti}_2\text{O}_7$, (c) spinel type $(\text{Cr}, \text{Mn}, \text{Fe}, \text{Co}, \text{Ni})_3\text{O}_4$, and (d) perovskite type $\text{La}(\text{Cr}, \text{Mn}, \text{Fe}, \text{Co}, \text{Ni})\text{O}_3$.

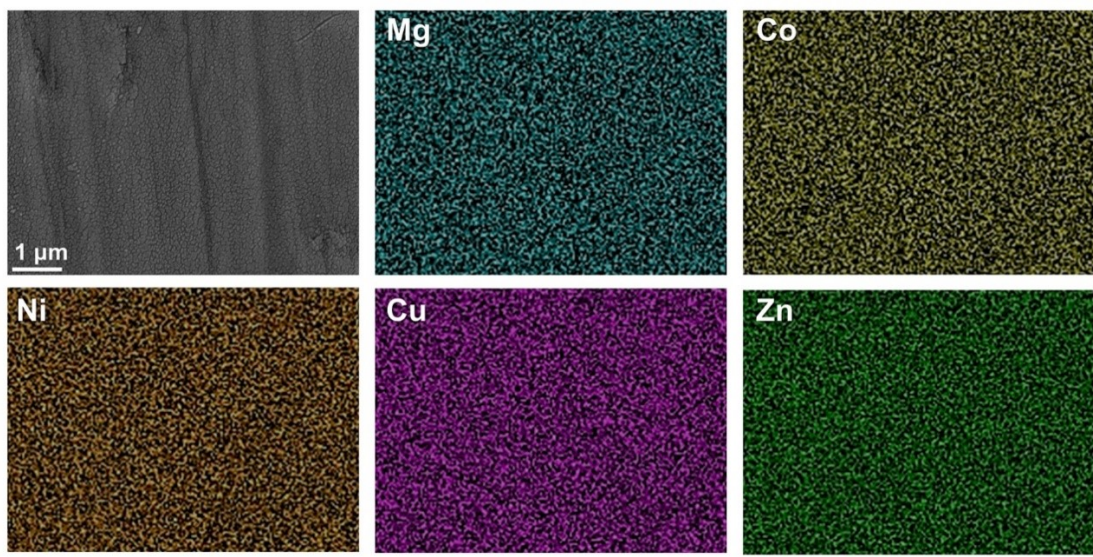


Fig. S2 EDS-SEM elemental maps of Mg, Co, Ni, Cu and Zn for rock-salt type $(\text{Mg},\text{Co},\text{Ni},\text{Cu},\text{Zn})\text{O}$ HEO.

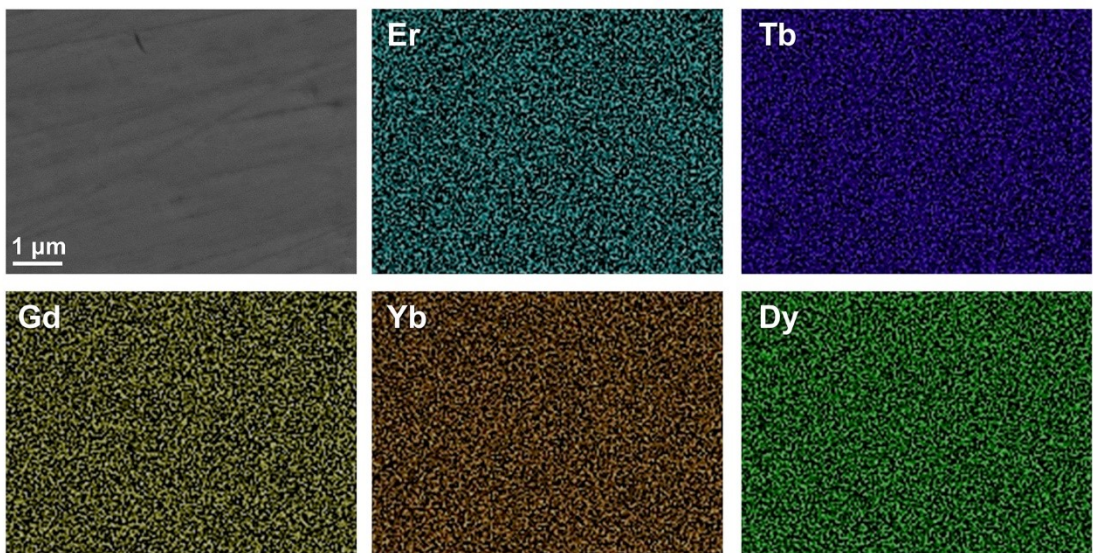


Fig. S3 EDS-SEM elemental maps of Er, Tb, Gd, Yb and Dy for pyrochlore type $(\text{Yb},\text{Tb},\text{Gd},\text{Dy},\text{Er})_2\text{Ti}_2\text{O}_7$ HEO.

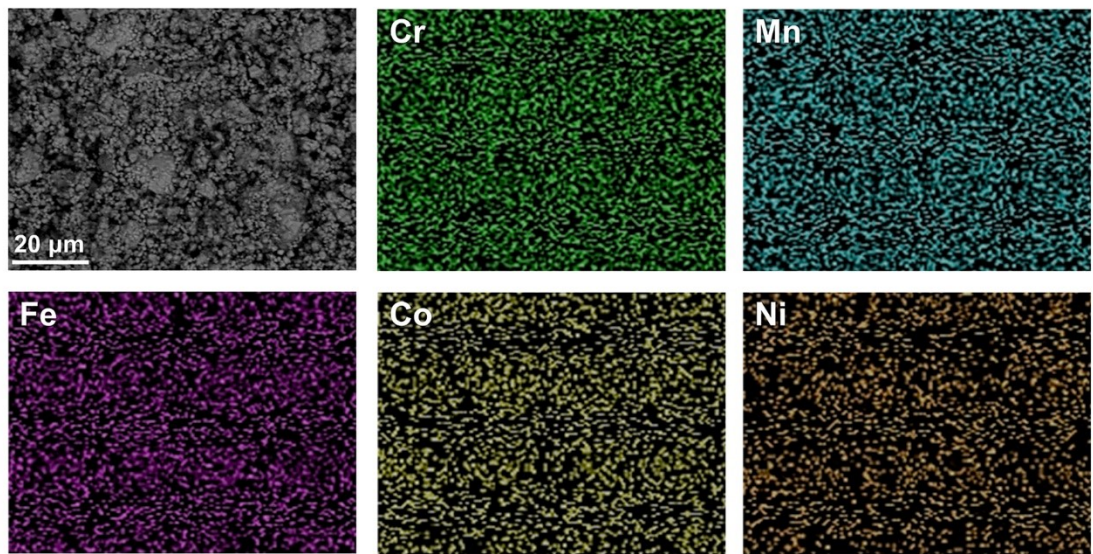


Fig. S4 EDS-SEM elemental maps of Cr, Mn, Fe, Co and Ni for spinel type $(\text{Cr},\text{Mn},\text{Fe},\text{Co},\text{Ni})_3\text{O}_4$ HEO.

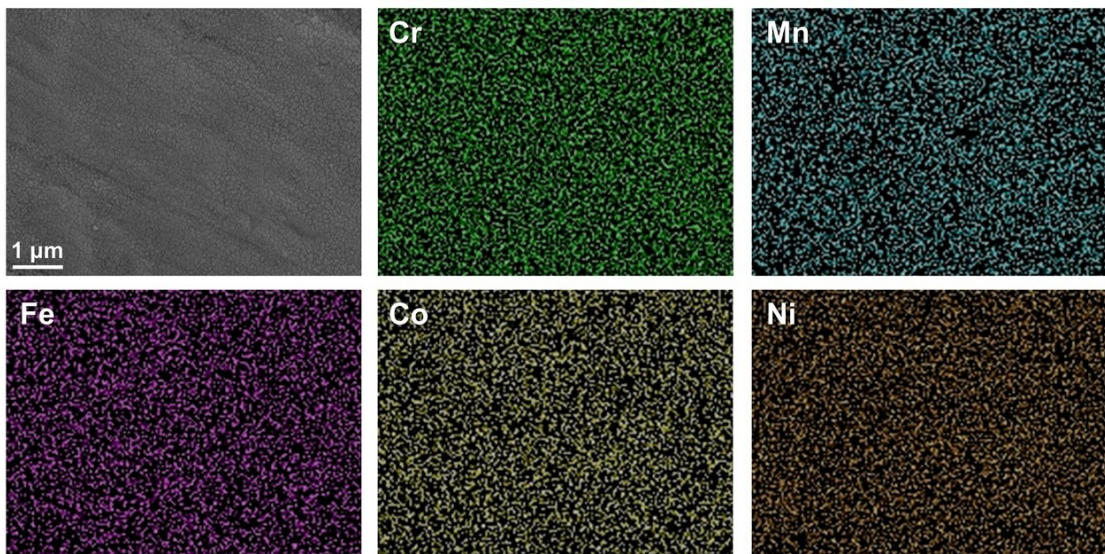


Fig. S5 EDS-SEM elemental maps of Cr, Mn, Fe, Co and Ni for perovskite type $\text{La}(\text{Cr},\text{Mn},\text{Fe},\text{Co},\text{Ni})\text{O}_3$ HEO.

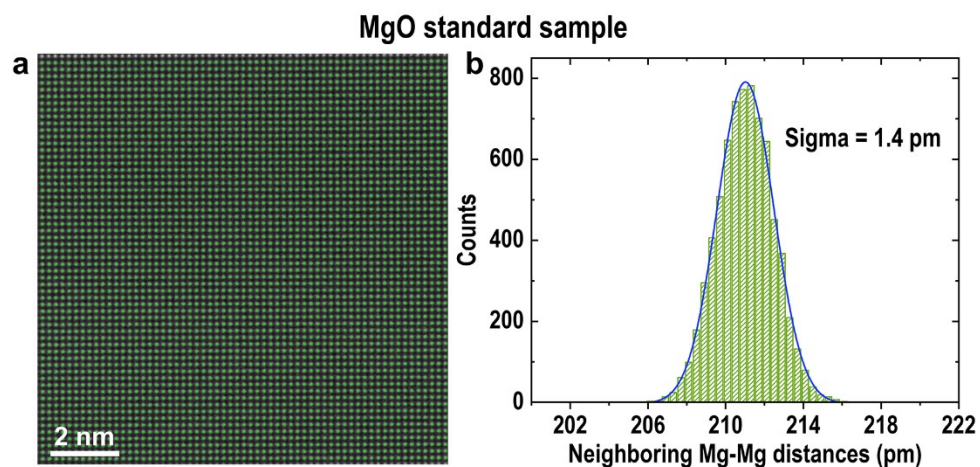


Fig. S6 Precision of atomic position fits estimated from the MgO standard sample. **(a)** The positions of atomic columns obtained by 2D Gaussian fits. **(b)** Histogram of distances between neighboring Mg atomic columns. The Gaussian fits for this histogram show Sigma (precision) is 1.4 pm.

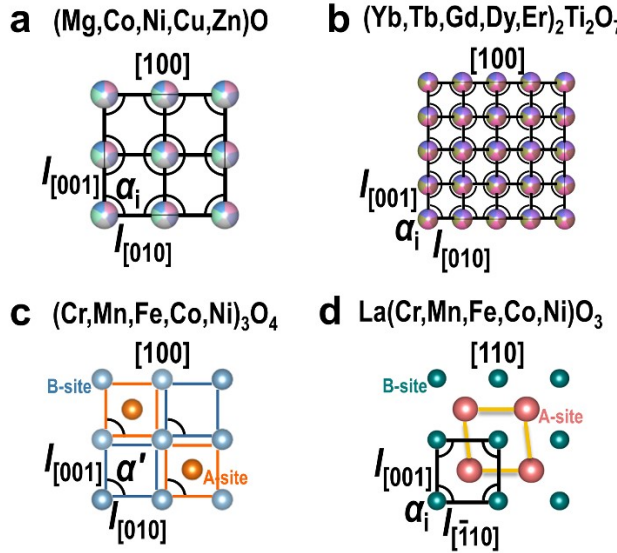


Fig. S7 Quantification methods of aspect ratios and inner angle variations from 90° for all quadrangle units in HAADF images of the four types of HEOs. Side lengths and inner angles for a quadrangle unit in (a) rock-salt type $(\text{Mg},\text{Co},\text{Ni},\text{Cu},\text{Zn})\text{O}$ and (b) pyrochlore type $(\text{Yb},\text{Tb},\text{Gd},\text{Dy},\text{Er})_2\text{Ti}_2\text{O}_7$ HEOs. The aspect ratio for a quadrangle unit

$$\frac{l_{[001]}^{\text{left}} + l_{[001]}^{\text{right}}}{l_{[010]}^{\text{up}} + l_{[010]}^{\text{down}}}$$

is calculated based on $\frac{l_{[010]}^{\text{up}} + l_{[010]}^{\text{down}}}{l_{[001]}^{\text{left}} + l_{[001]}^{\text{right}}}$. (c) Side lengths and inner angles for a quadrangle unit in the spinel type $(\text{Cr},\text{Mn},\text{Fe},\text{Co},\text{Ni})_3\text{O}_4$ HEO. The aspect ratio and inner angle

$$\frac{l_{[001]}}{l_{[010]}}$$

deviation parameter from 90° for a quadrangle unit are calculated based on $\frac{l_{[010]}}{l_{[001]}}$ and $\alpha = \alpha' - 90^\circ$, respectively. (d) Side lengths and inner angles for a quadrangle unit in the perovskite type $\text{La}(\text{Cr},\text{Mn},\text{Fe},\text{Co},\text{Ni})\text{O}_3$. The aspect ratio and inner angle deviation

$$\frac{l_{[001]}^{\text{left}} + l_{[001]}^{\text{right}}}{l_{[110]}^{\text{up}} + l_{[110]}^{\text{down}}}$$

parameter from 90° for a quadrangle unit are calculated based on $\frac{l_{[110]}^{\text{up}} + l_{[110]}^{\text{down}}}{l_{[001]}^{\text{left}} + l_{[001]}^{\text{right}}}$ and

$$\frac{\sum_i^4 |\alpha_i - 90^\circ|}{4}$$

, respectively.

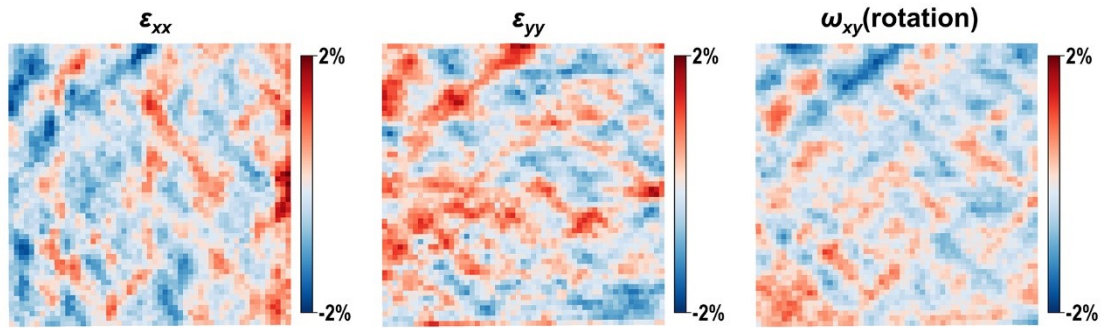


Fig. S8 Real-space strain analysis for Fig. 2(a) with uniaxial strain component ε_{xx} and ε_{yy} and rotation ω_{xy} maps for the rock-salt type $(\text{Mg},\text{Co},\text{Ni},\text{Cu},\text{Zn})\text{O}$ HEO.

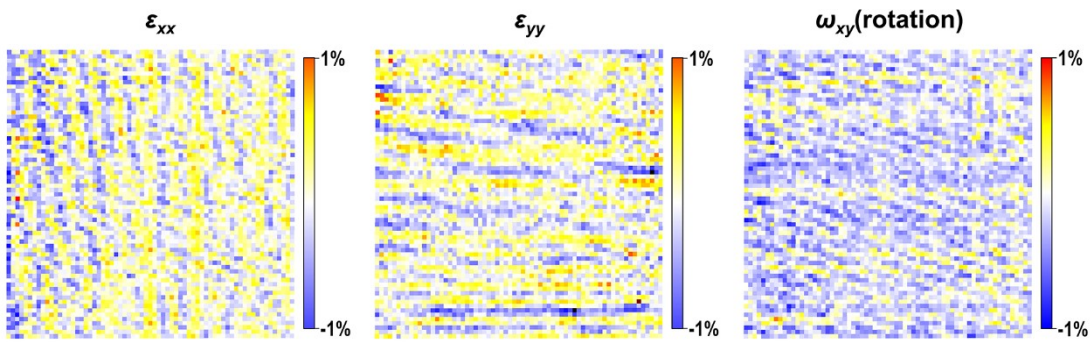


Fig. S9 Real-space strain analysis for Fig 3(a) with uniaxial strain component ε_{xx} and ε_{yy} and rotation ω_{xy} maps for pyrochlore type $(\text{Yb}, \text{Tb}, \text{Gd}, \text{Dy}, \text{Er})_2\text{Ti}_2\text{O}_7$ HEO.